Crystal Structure of the D94S/G98E Variant of Rat α-Parvalbumin. An Explanation for the Reduced Divalent Ion Affinity†

John J. Tanner,‡,§ Sayeh Agah,§,|| Yong-Hwan Lee,‡,⊥ and Michael T. Henzl*,§

Department of Chemistry, University of Missouri, Columbia, Missouri 65211, and Department of Biochemistry, University of Missouri, Columbia, Missouri 65211

Received April 27, 2005

ABSTRACT: Simultaneous replacement of Asp-94 with serine and Gly-98 with glutamate in rat α-parvalbumin creates a CD-site ligand array in the context of the EF-site binding loop. Previous work has shown that, relative to the wild-type CD site, this engineered site has markedly reduced Ca^{2+} affinity. Seeking an explanation for this phenomenon, we have obtained the crystal structure of the α D94S/G98E variant. The Ca^{2+} coordination within the engineered EF site of the 94/98E variant is nearly identical to that within the CD site, suggesting that the attenuated affinity of the EF site in 94/98E is not a consequence of suboptimal coordination geometry. We have also examined the divalent ion binding properties of the α 94/98E variant in both Na^+- and K^+-containing buffers. Although the Ca^{2+} and Mg^{2+} affinities are higher in K^+ solution, the increases are comparable to those observed for wild-type α. Consistent with that finding, the apparent Na^+ stoichiometry, estimated from stability studies conducted as a function of Na^+ concentration, is 1.0 ± 0.1, identical to that of wild-type α. Thus, the reduced affinity for divalent ions is evidently not the result of heightened monovalent ion competition. The thermodynamic analysis indicates that the less favorable Gibbs free energy of binding reflects a substantial enthalpic penalty. Significantly, the crystal structure reveals a steric clash between Phe-57 and the C_γ atom of Glu-98. The consequent displacement of Phe-57 also produces a close contact with Ser-55. Thus, steric interference may be the source of the enthalpic penalty.

Although Ca^{2+} fulfills several vital extracellular functions, notably in bone formation and blood coagulation, contemporary Ca^{2+} research is focused largely on its intracellular role in signal transduction. Supplied with an appropriate stimulus, virtually any eukaryotic cell will exhibit transient increases in cytosolic Ca^{2+} concentration, from a resting-state level between 20 and 100 nM to a maximum approaching 1 μM (*1*, *2*). These Ca^{2+} signals regulate myriad cellular processes, achieving specificity through spatial and temporal variations. Ca^{2+} exerts its influence through interactions with a multitude of Ca^{2+}-binding proteins. Many of these belong to the EF-hand protein family, named for its characteristic metal ion-binding motif (*3*−*5*). Certain EF-hand proteins, notably, calmodulin and troponin C, play overt regulatory roles. Others, notably calbindin and parvalbumin, serve as cytosolic Ca^{2+} buffers, modulating the amplitude and duration of the Ca^{2+} signals.

The 30-residue EF-hand motif consists of a 12-residue ion-binding loop flanked by short helical segments. Within the central loop, the liganding moieties are arrayed in pseudo-octahedral fashion around the bound ion and, accordingly, are indexed by a Cartesian coordinate system ($+x$, $+y$, $+z$, $-y$, $-x$, and $-z$). The $-y$ position is occupied by a main-chain carbonyl; the $-x$ ligand is frequently a water molecule, and the $-z$ ligand is a nearly invariant glutamyl residue. The remaining ligands are side-chain oxygen atoms (carboxylate, carbonyl, or hydroxyl). The coordination sphere typically contains three or four carboxylates. Because the $-z$ glutamate binds Ca^{2+} in a bidentate manner, the coordination is actually pentagonal bipyramidal. The $+y$, $+z$, $-y$, and $-z$ ligands lie in the equatorial plane, and the $+x$ and $-x$ species contribute the axial ligands.

Despite their general overall similarity, EF-hand motifs exhibit a broad range of divalent ion affinities. It is increasingly evident that the metal ion binding properties of a particular EF-hand site are influenced by local- and long-range structural features. For example, binding site I in calmodulin and the EF site[1] of parvalbumin have identical inner coordination spheres, consisting of three aspartyl

† This work was supported by NSF Grant MCB0131166 (to M.T.H. and J.J.T.).

* To whom correspondence should be addressed. Telephone: (573) 882-7485. Fax: (573) 884-4812. E-mail: henzlm@missouri.edu.

‡ Department of Chemistry.

§ Department of Biochemistry.

|| Present address: Department of Orthopedic Surgery, University of California, Los Angeles, CA 90095-6902.

⊥ Present address: Department of Biological Sciences, Louisiana State University, Baton Rouge, LA 70803.

[1] Abbreviations: CD, circular dichroism; CD site, parvalbumin metal ion-binding site flanked by the C and D helical segments; DSC, differential scanning calorimetry; EDTA, ethylenediaminetetraacetic acid; EF site, parvalbumin metal ion-binding site flanked by the E and F helical segments; EGTA, ethylene glycol bis(β-aminoethyl ether)-*N*,*N*,*N*′,*N*′-tetraacetic acid; Hepes, 4-(2-hydroxyethyl)-1-piperazineethanesulfonic acid; ITC, isothermal titration calorimetry; LB, Luria-Bertani; NMR, nuclear magnetic resonance; P_i, phosphate; PV, parvalbumin; 94/98, parvalbumin variant in which Asp-94 has been replaced with serine and Gly-98 has been replaced with either aspartate (94/98D) or glutamate (94/98E).

10.1021/bi050770t CCC: $30.25
Published on Web 07/26/2005

carboxylates (+*x*, +*y*, +*z*), a backbone carbonyl (−*y*), a water molecule (−*x*), and the bidentate glutamyl carboxylate (−*z*). Nevertheless, their apparent Ca^{2+} association constants differ by nearly 4 orders of magnitude. The basis for this disparity is now reasonably well understood. Specifically, the binding of Ca^{2+} to calmodulin, but not parvalbumin, provokes an energetically costly solvent exposure of apolar surface area.

A detailed appreciation of integrated Ca^{2+} signaling activity requires a comprehensive understanding of the kinetics and thermodynamics of the relevant Ca^{2+} pumps, channels, and binding proteins. For nearly three decades, investigators have sought to identify the physical basis for variations in EF-hand divalent ion affinity. This effort is complicated by the profound influence of higher-order structural considerations. Our work in this area has focused on structure−affinity relationships in the parvalbumin family.

Parvalbumins are small (M_r = 12 000) vertebrate-specific proteins believed to act as cytosolic Ca^{2+} buffers (*6*, *7*). They contain two Ca^{2+}-binding sites, the CD and EF sites, named for the helical segments flanking the ion-binding loops. In fact, the "EF-hand" motif is named after the EF site in carp parvalbumin, where it was first observed (*8*). The parvalbumin (PV) family includes two sublineages, α and *β*, that can be distinguished on the basis of isoelectric point, C-terminal helix length, and lineage-specific sequence eccentricities (*9*, *10*). Mammals express one isoform from each lineage (*11*). Although the sequences of the two proteins from rat are 49% identical (*12*, *13*), they exhibit disparate divalent ion binding properties. In 0.15 M KCl and 0.025 M Hepes-KOH (pH 7.4), the binding of Ca^{2+} is 5.5 kcal/mol more favorable for α (*14*).

As part of an inquiry into the basis for this disparate behavior, we produced and characterized a series of "site-interconversion" variants in both the rat α and *β* backgrounds (*15*−*17*). The ligand arrays in the parvalbumin CD and EF sites differ at the +*z* and −*x* positions: serine and glutamate (aspartate in *β*) in the CD site and aspartate and glycine in the EF site, respectively. The combined S55D and E59G (D59G in *β*) mutations produce an EF-like array in the confines of the CD site. Conversely, the D94S and G98E (G98D in *β*) mutations produce a CD-like site in the confines of the EF site. The impact of these mutations has been discussed at length elsewhere (*16*, *17*). Significantly, the 94/98 mutations markedly decrease the EF-site Ca^{2+} affinity, regardless of whether they are made in α or *β* or whether Gly-98 is replaced with aspartate or glutamate. Because the basis for this effect was unclear, we have obtained high-resolution structural data on the α D94S/G98E variant and extended our previous metal ion binding studies. The results of this work offer insight into the divalent ion binding behavior of the 94/98 variants.

MATERIALS AND METHODS

Protein Purification. α 94/98 was isolated by a minor modification of the procedure described previously for wild-type α (*18*, *19*). Protein concentrations were determined spectrophotometrically, employing an extinction coefficient at 258 nm of 1600 M^{-1} cm^{-1}. Residual divalent metal ions were removed from protein solutions and buffers when they were passed over a column of EDTA−agarose (*20*), prepared as described elsewhere (*21*). Protein preparations thus treated contained <0.02 equiv of Ca^{2+}, as determined by flame atomic absorption spectrometry.

Table 1: Data Collection and Refinement Statistics[a]

PDB entry	1XVJ
space group	$P2_1$
unit cell parameters	a = 30.7 Å, b = 57.0 Å, c = 56.5 Å, β = 105.8°
no. of crystals	1
no. of protein molecules in the asymmetric unit	2
diffraction resolution (Å)	25−1.8 (1.85−1.80)
no. of observations	50844
no. of unique reflections	16037
completeness (%)	92 (90)
mean I/σ_I	25.3 (9.6)
R_{merge}	0.066 (0.224)
no. of protein atoms	1653
no. of calcium ions	4
no. of water molecules	199
R_{cryst}	0.197 (0.261)
R_{free}[b]	0.236 (0.348)
rmsd[c]	
bond lengths (Å)	0.010
bond angles (deg)	1.2
Ramachandran plot[d]	
favored (%)	93.9
allowed (%)	6.1
generously allowed (%)	0.0
disallowed (%)	0.0
average *B*-factors (Å^2)	
protein	17
calcium ions	15
solvent	22

[a] Values for the outer resolution shell of data are given in parentheses. [b] The 5% R_{free} test set. [c] Compared to the Engh and Huber force field (*32*). [d] The Ramachandran plot was generated with PROCHECK (*35*).

X-ray Crystallography. Crystals of α 94/98E were grown by the hanging-drop vapor-diffusion method. Equal volumes of protein solution (40 mg/mL) and precipitant [30% PEG 550 MME, 0.10 M Mes (pH 6.5), 0.01 M $ZnSO_4$, and 0.001 M $CaCl_2$] were combined and incubated at 21 °C. The resulting crystals grew in space group $P2_1$, with two molecules per asymmetric unit, 37% solvent content, and a Matthews coefficient of 2.0 (*22*). The unit cell parameters are as follows: a = 30.7 Å, b = 57.0 Å, c = 56.5 Å, and β = 105.8°. A 1.8 Å data set was collected from a single crystal, employing an R-axis IV detector. X-rays were produced with a Rigaku RU-H3R copper rotating-anode generator, equipped with Osmic MaxFlux confocal optics and an X-stream cryogenic system. The data were processed with *HKL* (*23*), and the reflection intensities were converted to amplitudes using the method of French and Wilson (*24*), as implemented in CCP4 (*25*). The structure was determined by molecular replacement with CNS (*26*). The search model employed the coordinates for the 1.05 Å wild-type rat α-parvalbumin structure [PDB entry 1RWY (*27*)], omitting residues within 3.9 Å of residue 94 or residue 98, to minimize model bias. Refinement was conducted with CNS and REFMAC5 (*28*), and model building was conducted with O (*29*). Data collection and processing statistics are presented in Table 1.

PDB Entry. The atomic coordinates and structure factors have been deposited in the Protein Data Bank as entry 1XVJ.

Ca^{2+} and Mg^{2+} binding affinities were determined by global analysis of isothermal titration calorimetry (ITC) data. Samples of α 94/98 were titrated with Ca^{2+}, with Mg^{2+}, with Ca^{2+} in the presence of Mg^{2+}, with Ca^{2+} in the presence of competitive chelators (EDTA and EGTA), and with Mg^{2+} in the presence of EDTA. The resulting data were compiled into a master file and analyzed by nonlinear least-squares minimization, as described elsewhere (*14*, *30*). The reported uncertainties are the 68% confidence intervals. The ITC experiments were conducted in a VP-ITC instrument (MicroCal) at 25 °C, either in 0.15 M NaCl and 0.025 M Hepes-NaOH (pH 7.4) or in 0.15 M KCl and 0.025 M Hepes-KOH (pH 7.4).

Estimation of the α D94S/G98E Na^+ Binding Constants by Monte Carlo Simulation. The apparent Ca^{2+} binding constants measured in K^+ or Na^+ solution were used to produce synthetic Ca^{2+} binding data for the two buffer conditions. Estimates of the Na^+ affinity constants for α 94/98E were obtained by Monte Carlo analysis, employing a model that included M, MX, MX_2, MY, and MXY, where M represents the macromolecule, X represents Ca^{2+}, and Y represents Na^+. In the presence of Na^+, the extent of divalent ion binding for this system after the *i*th addition, $\bar{X}_i$, is described by

$$\bar{X}_i = [K_{10}(1 + K_{11}Y_i)X_i + 2K_{20}K_{10}X_i^2]/P \quad (1)$$

where P is the partition function

$$P = 1 + K_{01}Y_i + K_{10}(1 + K_{11}Y_i)X_i + K_{20}K_{10}X_i^2 \quad (2)$$

In eqs 1 and 2, X_i and Y_i are the free Ca^{2+} and Na^+ concentrations, respectively, after the *i*th addition, K_{10} and K_{20} are the true macroscopic association constants for the first and second divalent ion binding events, respectively (i.e., unperturbed by Na^+), K_{01} is the Na^+ binding constant for the apoprotein, and K_{11} is the corresponding constant for the MX species. Because Na^+ was present in such large excess, X_i was fixed at the total Na^+ concentration.

The Ca^{2+} binding constants measured in K^+ solution provided values for K_{10} and K_{20}. The corresponding analysis of the wild-type protein, reported previously (*14*), provided starting estimates for the Na^+ binding constants, K_{01} and K_{11}. After calculation of the initial χ^2 value, a new parameter set was generated by incrementing K_{01} and K_{11} by an arbitrary quantity, ΔK. The magnitude of ΔK is equal to the output from a random number generator multiplied by some arbitrary fraction of the initial parameter value. χ^2 was then recalculated. Simulations were performed both with and without minimization, until values of K_{01} and K_{11} were identified that brought the calculated binding curve in the presence of Na^+ into agreement with the observed one.

Circular Dichroism. The denaturation of α 94/98E was monitored by CD as a function of Na^+ concentration. Prior to analysis, samples were dialyzed to equilibrium against 0.005 M sodium phosphate and 0.01 M EDTA (pH 7.4) containing various concentrations of NaCl. The CD signal at 222 nm was acquired with an Aviv 62DS spectrometer on each sample at 0.25 °C intervals between 5 and 90 °C. The samples, having nominal concentrations of 0.8 mg/mL, were contained in sealed quartz cuvettes (0.1 cm path length). Estimates of the melting temperature and denaturational enthalpy were obtained by fitting the resulting data to this equation:

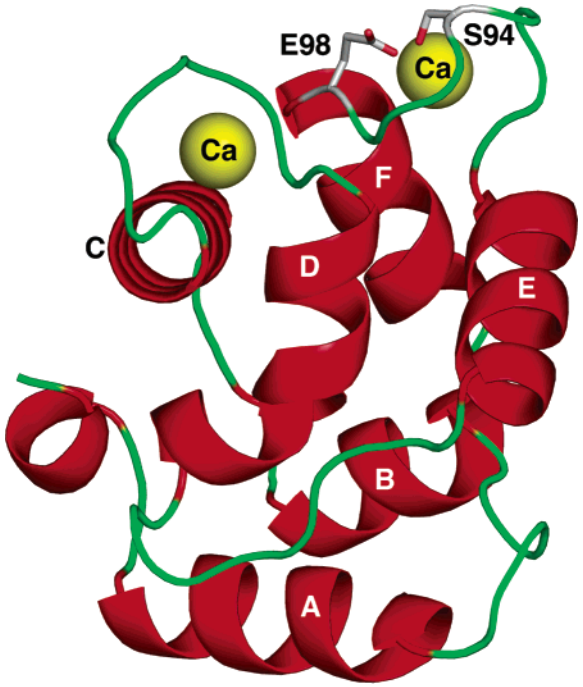

FIGURE 1: Ribbon drawing of the D94S/G98E variant of rat α-PV. The α-helices are labeled A−F, and side chains of Ser-94 and Glu-98 are drawn in ball-and-stick mode. Figures 1−4 were prepared with PyMol (*36*).

$$y = \frac{(y_f + m_f T) + (y_u + m_u T)\exp\{(\Delta H_u/RT)[(T - T_m)/T_m]\}}{1 + \exp\{(\Delta H_u/RT)[(T - T_m)/T_m]\}} \quad (3)$$

where y is the raw ellipticity signal, m_f, y_f, m_u, and y_u represent the slope and intercept, respectively, for the pre- and post-transition baselines, ΔH is the apparent, or van't Hoff, enthalpy for denaturation, R is the gas constant, and T_m is the absolute melting temperature (*31*). The reversibility of α 94/98E denaturation has been demonstrated previously by DSC; i.e., the area of the endotherm obtained when the sample is rescanned is comparable to that of the original scan.

RESULTS

X-ray Crystallography. D94S/G98E displays the well-known parvalbumin fold, consisting of three pairs of α-helices (labeled A−F) organized into two domains (Figure 1). The A and B helices and the broad connecting loop comprise the N-terminal AB domain. Helices C−F form a classical EF-hand Ca^{2+}-binding domain, i.e., two of the distinctive helix−loop−helix motifs related by a 2-fold symmetry axis. Ca^{2+} ions occupy their expected positions in the loops connecting the C−D and E−F helical pairs. The two protein molecules in the asymmetric unit exhibit virtually identical structures, with root-mean-square differences (rmsds) of 0.3 Å for backbone atoms and 0.6 Å for all atoms. The backbone rmsds for the CD and EF Ca^{2+}-binding loops are just 0.1 and 0.3 Å, respectively.

Residues 94 and 98 occur in the Ca^{2+}-binding loop of the EF site (Figure 1). The simultaneous replacement of Asp-94 with serine and Gly-98 with glutamate effectively

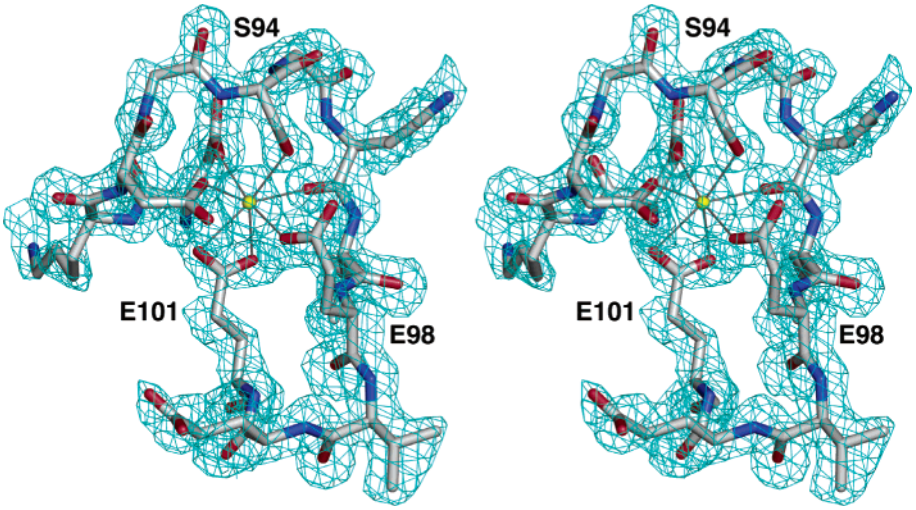

FIGURE 2: Stereoview of the EF site of chain B covered by a σ_A-weighted simulated annealing $F_o - F_c$ map (2.5σ). Prior to calculation of the map, residues 90−101 and the calcium ion of the EF site were omitted, and simulated annealing refinement was performed.

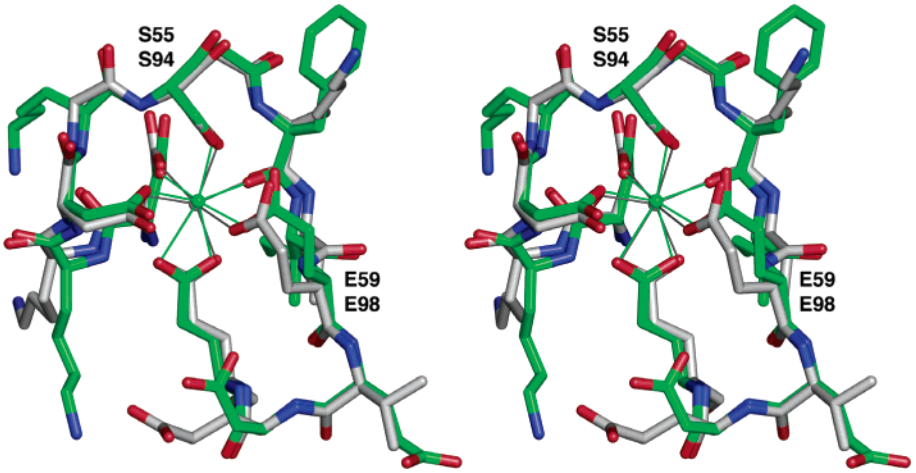

FIGURE 3: Stereoview of the CD Ca^{2+}-binding site of α D94S/G98E (green) superimposed on the EF site (white). Bonds to the calcium ions are shown as solid lines.

transplants the CD-site ligand array into the EF site, with Ser-94 and Glu-98 in the engineered site assuming the roles played by Ser-55 and Glu-59, respectively, in the CD site. This structural analysis of D94S/G98E was undertaken to ascertain whether the constellation of ligands found in the CD Ca^{2+}-binding site is compatible with the structural and energetic context of the EF domain.

The conformations of Ser-94 and Glu-98 were readily apparent from our initial 1.8 Å resolution electron density maps calculated after molecular replacement and rigid body refinement, and from the simulated annealing omit maps calculated from the final refined structure (Figure 2). Both residues coordinate the bound Ca^{2+} ion through side-chain oxygen atoms. The hydroxyl of Ser-94 occupies the $+z$ position; the carboxylate of Glu98 occupies the $-x$ position and interacts in a monodentate manner with the metal ion. These interactions are analogous to those formed by Ser-55 and Glu-59 in the CD site (Figure 3).

As anticipated, the bond lengths and angles of the 94/98E CD site are very similar to those in the wild-type CD site (Table 1). Interestingly, the Ca^{2+}-binding geometry in the engineered EF site of the variant is essentially indistinguishable from that observed for the CD site (Table 1). The largest discrepancy in bond length is just 0.2 Å ($-y$ position, Table 2), and the respective bond angles differ by less than 4° (Table 2).

As illustrated in Figure 3, the coordinating ligands in the mutated EF site (green) align closely with those in the CD site (white). Ser-94 is virtually coincident with Ser-55, and the ligating oxygen atoms of Glu-98 and Glu-59 likewise superimpose very well. These results indicate that the CD-site ligand array can, in fact, achieve optimal Ca^{2+} coordination geometry in the environs of the EF site. Evidently, the reduced affinity of the engineered EF site, relative to that of the CD site, is not a consequence of suboptimal Ca^{2+}-binding geometry. This unexpected finding suggests that the structural and energetic basis for the decreased binding free energy accrues from indirect effects originating outside of the coordination sphere.

Both mutations perturb their immediately adjacent surroundings. To bring the Ser-94 hydroxyl group within bonding distance of Ca^{2+} ion, the peptide backbone of residues 93−95 must shift by 0.2−0.7 Å. This movement occurs with minimal disruption of the surrounding structure, consistent with the structural context of residue 94. Located on the protein surface, residue 94 is largely free of noncovalent interactions with the neighboring polypeptide. It is also flanked by glycine residues, which impart flexibility to

Table 2: Ca^{+2} Binding Geometry of Rat α-Parvalbumin D94S/G98E Determined at 1.8 Å Resolution

Ca^{2+}−Ligand Distances (Å)					
		CD Site			
position	coordinating atom	*A*	*B*	average	wild-type value[a]
+*x*	Asp-51 OD1	2.33	2.36	2.34	2.27
+*y*	Asp-53 OD1	2.35	2.32	2.33	2.32
+*z*	Ser-55 OG	2.54	2.40	2.47	2.53
−*y*	Phe-57 O	2.31	2.26	2.28	2.33
−*x*	Glu-59 OE1	2.40	2.46	2.43	2.36
−*z*	Glu-62 OE1	2.46	2.43	2.44	2.42
−*z*	Glu-62 OE2	2.60	2.55	2.57	2.52
		EF Site			
+*x*	Asp-90 OD1	2.32	2.35	2.33	2.32
+*y*	Asp-92 OD1	2.37	2.37	2.37	2.35
+*z*	Ser-94 OG	2.47	2.49	2.48	2.34
−*y*	Lys-96 O	2.46	2.49	2.47	2.36
−*x*	Glu-98 OE2	2.35	2.29	2.32	2.40
−*z*	Glu-101 OE1	2.43	2.42	2.42	2.44
−*z*	Glu-101 OE2	2.61	2.46	2.53	2.53

Ligand−Ca^{2+}−Ligand Angles (deg)						
	CD site		*A*	*B*	average	wild-type value[a]
Asp-51 OD1	Ca^{2+}	Glu-59 OE1	168.3	170.9	169.6	166.1
Asp-53 OD1	Ca^{2+}	Glu-62 OE2	74.4	72.1	73.2	74.0
Ser-55 OG	Ca^{2+}	Asp-53 OD1	80.7	77.2	78.9	79.1
Phe-57 O	Ca^{2+}	Ser-55 OG	75.1	79.5	77.3	75.6
Glu-62 OE1	Ca^{2+}	Phe-57 O	80.4	80.9	80.6	80.2
	EF site		*A*	*B*	average	wild-type value[a]
Asp-90 OD1	Ca^{2+}	Glu-98 OE2	173.6	168.9	171.2	161.3
Asp-92 OD1	Ca^{2+}	Glu-101 OE2	73.8	76.3	75.0	75.1
Ser-94 OG	Ca^{2+}	Asp-92 OD1	78.0	82.8	80.4	80.9
Lys-96 O	Ca^{2+}	Ser-94 OG	77.9	69.6	73.7	79.5
Glu-101 OE1	Ca^{2+}	Lys-96 O	81.0	79.7	80.3	81.9

[a] Values for the wild-type protein were obtained from the 1.05 Å rat α-parvalbumin structure.

this region and allow the chain to easily flex inward toward the ion (Figure 1).

Residue 98, by contrast, is proximal to the interface between the CD and EF sites (Figures 1 and 4A) and thus experiences more structural and energetic constraints. In wild-type rat α, the C_α atom of Gly-98 is positioned just 3.6−3.8 Å from the Phe-57 side chain. Phe-57, in turn, is highly constrained by its local environment. C_β contacts the carboxylate group of Glu-59 (3.5 Å), and the phenyl ring is sandwiched between the carbonyl oxygen of Ser-55 (3.6 Å) on one face and Lys-96 (3.5−3.8 Å) on the other. This close packing severely restricts rotation around the Phe-57 χ_2 angle.

Mutation of Gly-98 to glutamate causes a subtle, yet energetically significant, change in the conformation of Phe-57. Relative to the wild-type structure, Phe-57 has rotated 8−14° about the χ_1 angle (Figure 4B). This rotation is necessitated by steric clashes of 3.5−3.7 Å between the side chain of Glu-98 and the phenyl ring of Phe-57 (Figure 4). The rotation of Phe-57, in turn, increases the close contact between the phenyl ring of Phe-57 and the carbonyl oxygen of Ser-55 (3.2−3.3 Å). Note that the contact distances between Glu-98 and Phe-57 (3.5−3.7 Å) are smaller than the Lennard-Jones σ parameter for this interaction [$\sigma = 3.9$ Å, based on σ values of CH2E and CR1E atom types (*32*)]. Thus, it appears that the 94/98 double mutation has increased the noncovalent potential energy of the Ca^{2+}-bound form of the protein by introducing close contacts at the interface between the two sites and within the CD site.

Divalent Ion Binding Behavior. The Ca^{2+} and Mg^{2+} binding properties of α 94/98 were measured by ITC in both Na^+- and K^+-containing buffers. Figure 5 presents raw data from titrations of the protein with Ca^{2+} (panel A) and Mg^{2+} (panel B) under the two solution conditions. As noted previously for wild-type α (*14*), solvent cation identity has a major impact on the divalent ion binding behavior α 94/98E. Consistent with preliminary measurements on this protein in Na^+ solution (*17*), whereas the first Ca^{2+} binding event is exothermic, the second is endothermic. Although qualitatively similar behavior is observed in the presence of K^+, the first binding event is profoundly more exothermic. Likewise, whereas Mg^{2+} binding is endothermic in the presence of Na^+, it is strongly exothermic in the presence of K^+.

Na^+ Solution. To determine the Ca^{2+} and Mg^{2+} binding constants in Na^+ solution, samples of the protein were titrated with Ca^{2+}, with Mg^{2+}, with Ca^{2+} in the presence of three fixed levels of Mg^{2+}, with Ca^{2+} in the presence of EDTA or EGTA, and with Mg^{2+} in the presence of EDTA. Integrated data from these eight experiments are presented in Figure 6. The apparent discontinuities in the titrations performed with Mg^{2+} result from doubling the injection volume in the latter stages of the titration.

Initial estimates for the Ca^{2+} binding parameters were obtained from analysis of the single Ca^{2+} titration shown in Figure 6A. The magnitude of the second Ca^{2+} binding constant, $\sim 10^5\ M^{-1}$, suggested that the corresponding Mg^{2+}

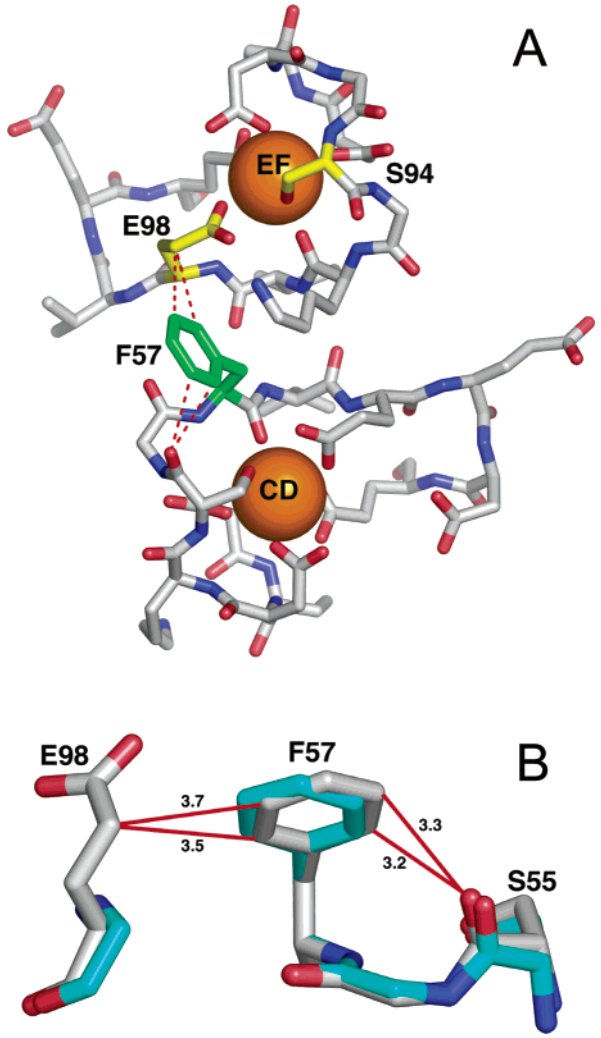

FIGURE 4: Steric interference between Glu-98 and Phe-57. (A) Drawing of the CD and EF Ca^{2+}-binding sites of D94S/G98E. Calcium ions are colored orange; Ser-94 and Glu-98 are colored yellow, and Phe-57 is colored green. The red dashed lines indicate close contacts involving Phe-57. Note that Glu-98 and Phe-57 are located in the interface between the CD and EF domains. (B) Superposition of the wild-type structure (cyan) onto D94S/G98E (white). The red lines indicate close contacts involving Phe-57. The numbers denote distances in angstroms.

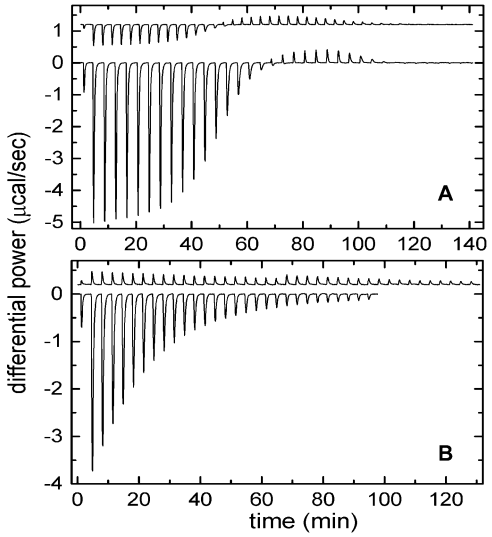

FIGURE 5: Representative raw ITC data in Na^+ and K^+ solutions. (A) The top trace, offset for clarity, corresponds to the titration of α 94/98E with Ca^{2+} in 0.15 M NaCl and 0.025 M Hepes-NaOH (pH 7.4). The bottom trace is the comparable experiment conducted in 0.15 M KCl and 0.025 M Hepes-KOH (pH 7.4). (B) The top trace corresponds to the titration of α 94/98E with Mg^{2+} in Na^+ solution. The bottom trace is from a similar experiment performed in K^+ solution.

constant would be on the order of 10 M^{-1}. A binding site with this minimal affinity would be negligibly populated under these experimental conditions. Accordingly, the data were treated with the assumption of a single Mg^{2+}-binding site. Initial parameter estimates for this site were obtained by fitting the Mg^{2+} titration shown in Figure 6D (○) with a one-site model. For the global fit, the binding constant for the second site was fixed at 1×10^{-5} M^{-1} and assigned a binding enthalpy of zero.

A satisfactory fit was obtained with the assumption of a single bound Mg^{2+} ion, as suggested by the solid lines through the data points in Figure 6A, C, E, and G as well as the patterns of residuals plotted in Figure 6B, D, F, and H. The minimized χ^2 value for the global fit was not significantly reduced by including a second Mg^{2+}-binding site. The resulting parameters are listed in Table 3. The Ca^{2+} binding constants determined by ITC (4.4×10^7 and 5.4×10^5 M^{-1}) are in reasonably good agreement with the values previously measured by $^{45}Ca^{2+}$ flow dialysis (*16*). That earlier study, it should be noted, did not include measurements in the presence of Mg^{2+}.

In wild-type α, the CD and EF sites behave indistinguishably in titrations with Ca^{2+} or Mg^{2+}. By contrast, the two sites in 94/98E are decidedly nonequivalent, with the Ca^{2+} binding constant for the engineered EF site nearly 2 orders of magnitude lower than that of the CD site. Thus, as previously noted (*16*, *17*), introduction of the CD ligand array into the EF site has markedly reduced divalent ion affinity and destroyed the functional equivalency of the two sites.

K^+ Solution. Samples of α 94/98 in 0.15 M KCl and 0.025 M Hepes (pH 7.4) were subjected to a battery of titrations similar to that described above. The integrated data from those experiments are displayed in Figure 7A, C, E, and G. In contrast to the data collected in Na^+ solution, a significant reduction in the χ^2 was achieved by including binding parameters for a second Mg^{2+}-binding site.

The optimal parameter values are listed in Table 3. As observed previously for wild-type α (*14*), divalent ion affinity is substantially increased when K^+ is the primary solvent cation. The first Ca^{2+} binding constant is increased by a factor of 4.4 and the second by a factor of 5.7. The first Mg^{2+} constant is also increased by a factor of 4.5. As mentioned earlier, it was not possible to extract a meaningful estimate for the second Mg^{2+} binding constant in Na^+ solution. If, however, one assumes that the increase in affinity in K^+ solution would parallel that observed for the second Ca^{2+} binding constant (i.e., a factor of 5.7), then the value in Na^+ would be on the order of 30 M^{-1}.

Rat α is less conformationally stable in K^+ solution, because of an inability of the larger monovalent ion to bind, and stabilize, the apoprotein. Whereas the T_m is 46 °C in 0.24 M Na^+, it is 35 °C in 0.24 M K^+ (*19*). The melting temperature of α 94/98E is approximately 3 °C lower than that of wild-type α in 0.24 M Na^+ (see below). Assuming a similar decrease in K^+ solution, the T_m would be roughly

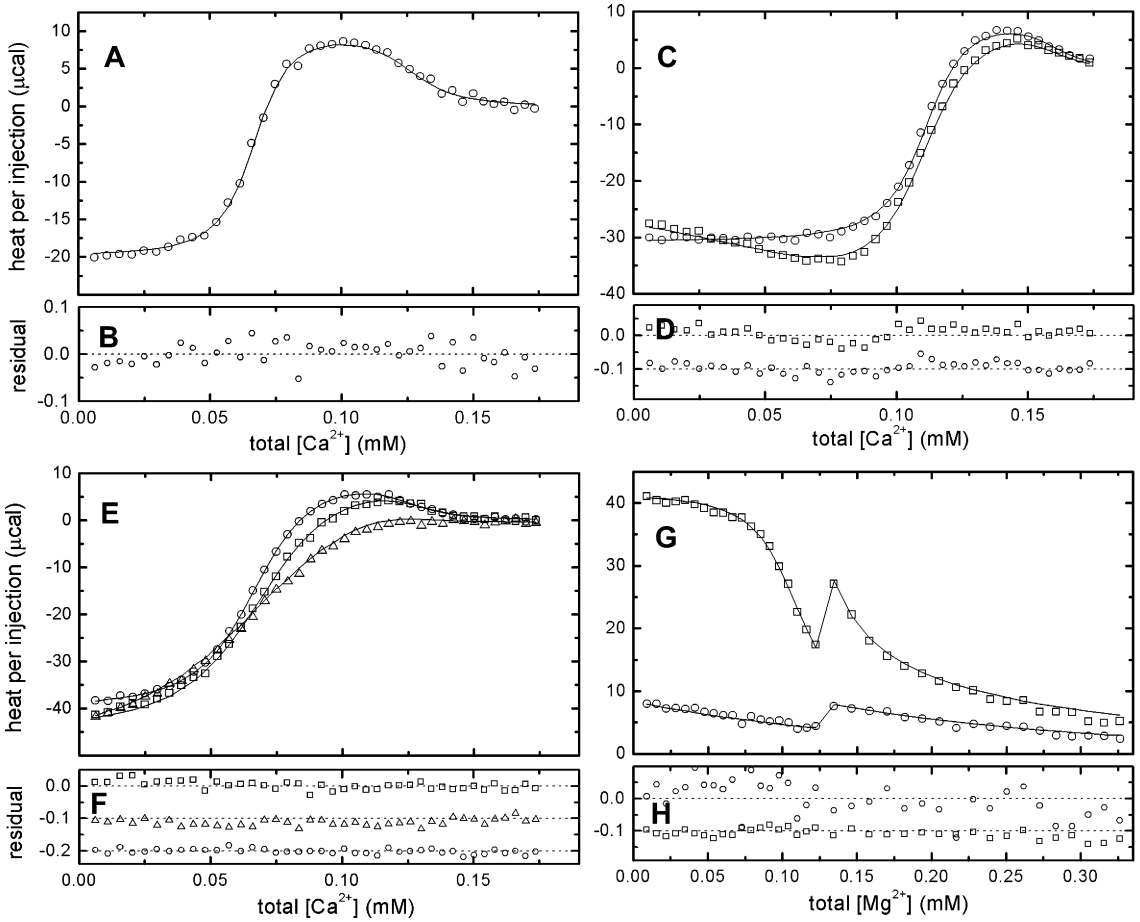

FIGURE 6: Integrated ITC data for the global analysis of α 94/98E divalent ion binding in Na^+ solution: (A) 0.96 mM Ca^{2+} vs 73 μM α 94/98E, 7 μL additions; (C) 0.96 mM Ca^{2+} vs 66 μM α 94/98E, 60 μM EDTA, 7 μL additions (○); 0.96 mM Ca^{2+} vs 66 μM α 94/98E, 60 μM EGTA, 7 μL additions (□); (E) 0.96 mM Ca^{2+} vs 72 μM α 94/98E, 0.50 mM Mg^{2+}, 7 μL additions (○); 0.96 mM Ca^{2+} vs 74 μM α 94/98E, 1.0 mM Mg^{2+}, 7 μL additions (□); 0.96 mM Ca^{2+} vs 71 μM α 94/98E, 3.0 mM Mg^{2+}, 7 μL additions (△); and (G) 1.84 mM Mg^{2+} vs 73 μM α 94/98E, 7 μL additions (○); 1.842 mM Mg^{2+} vs 72 μM α 94/98E, 110 μM EDTA, 7 μL additions (□). (B) Residuals for panel A. (D) Residuals for panel C. (F) Residuals for panel E. (H) Residuals for panel G. Residuals were scaled to the largest injection heat in each data set.

Table 3: Divalent Ion Binding Properties of α D94S/G98E in Na^+ and K^+ Solution[a]

	Ca^{2+} values				Mg^{2+} values			
solvent cation	k_1 (M^{-1})	ΔH_1 (kcal/mol)	k_2 (M^{-1})	ΔH_2 (kcal/mol)	k_{1M} (M^{-1})	ΔH_{1M} (kcal/mol)	k_{2M} (M^{-1})	ΔH_{2M} (kcal/mol)
Na^+	4.36×10^7	−2.96	5.35×10^5	1.55	3.77×10^3	4.80	−	−
	(4.05, 4.71)	(2.87, 3.07)	(4.82, 5.83)	(1.45, 1.64)	(3.47, 4.07)	(4.61, 4.99)		
K^+	1.95×10^8	−22.1	3.09×10^6	2.51	1.72×10^4	−14.4	153	2.26
	(1.80, 2.09)	(−22.6, −21.7)	(2.96, 3.36)	(2.30, 2.63)	(1.67, 1.79)	(14.1, 14.7)	(76, 228)	(0.84, 3.60)

[a] k_1 and k_2 are the first and second microscopic Ca^{2+} association constants, respectively; k_{1M} and k_{2M} are the values for Mg^{2+}, respectively.

32 °C. Thus, at 25 °C, the temperature of the binding study, a significant fraction of the protein would be unfolded. As a consequence, the apparent enthalpy of binding would include a contribution from protein folding. This linkage of metal ion binding and folding is responsible for the enhanced exothermicity associated with binding of divalent ion to 94/98E in K^+ solution.

Na^+ Binding Stoichiometry. The attenuation of α-PV divalent ion affinity in Na^+-containing solutions is believed to be the result of competition by the monovalent ion for the metal ion-binding loops. Wild-type rat α-PV binds 1 equiv of Na^+ with an estimated binding constant of 650 M^{-1}, and NMR data suggest that the bound Na^+ resides in the CD site of the apoprotein. Given that α 94/98 harbors two CD-like ligand arrays, we were interested in determining whether the apoprotein can bind 2 equiv of Na^+. Increased competition by the monovalent ion offered a potential explanation for the reduction in divalent ion affinity relative to that of the wild-type protein.

To address this issue, the thermal stability of 94/98E was examined as a function of Na^+ concentration. Samples of α 94/98 were examined by circular dichroism at 222 nm over the temperature range from 5 to 90 °C. The individual data sets (Figure 8A) were treated with eq 3, as described by Pace et al. (*31*), to extract estimates of the transition midpoints (T_m) and denaturational enthalpies (Table 4). The T_m values, listed in Table 4, have been plotted against the natural logarithm of the Na^+ concentration in Figure 8B. The data acquired at ≤0.44 M fall on a straight line, indicated by the dashed line in Figure 8B, with a slope of 3.44. However,

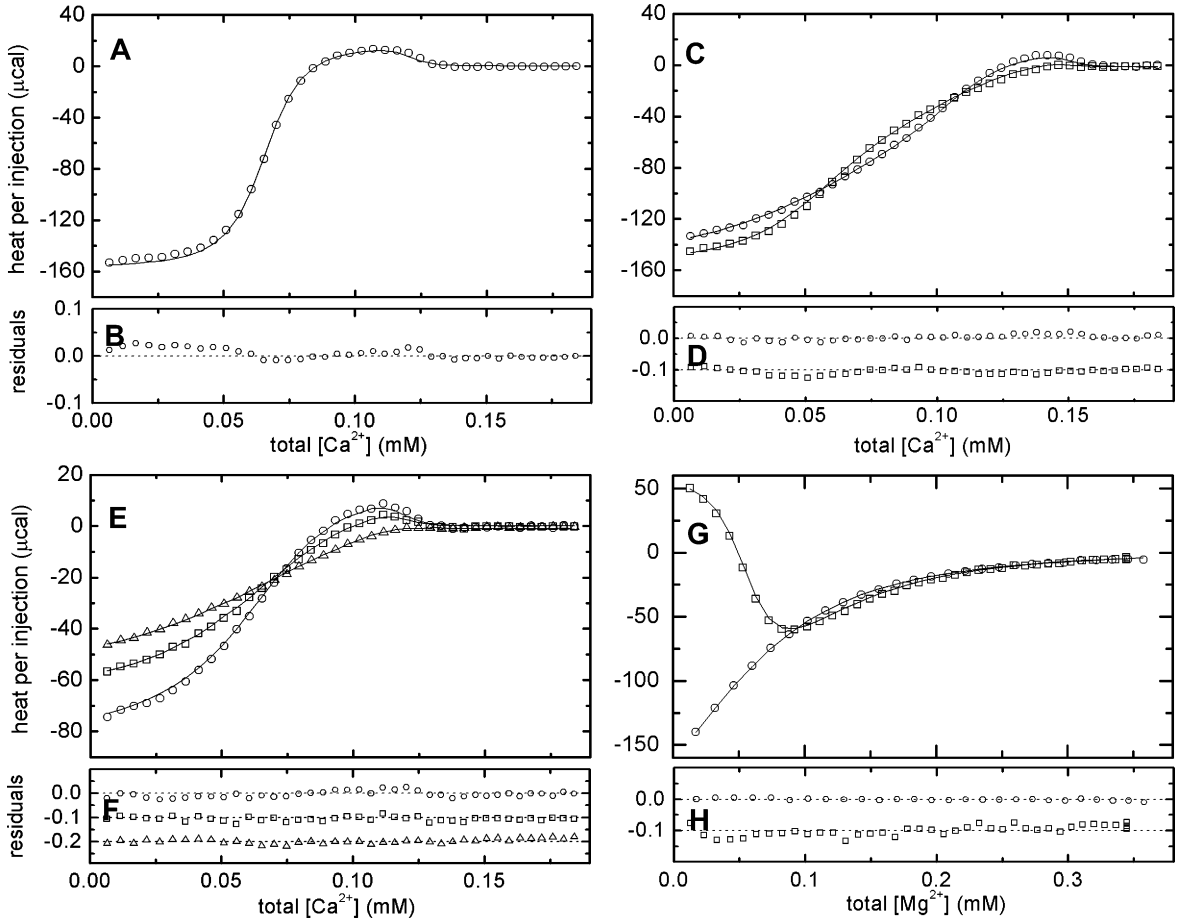

FIGURE 7: Integrated ITC data for the global analysis of α 94/98E divalent ion binding in K^+ solution: (A) 1.02 mM Ca^{2+} vs 68 μM α 94/98E, 7 μL additions; (C) 1.02 mM Ca^{2+} vs 56 μM α 94/98E, 54 μM EDTA, 7 μL additions (○); 1.02 mM Ca^{2+} vs 56 μM α 94/98E, 54 μM EGTA, 7 μL additions (□); (E) 1.02 mM Ca^{2+} vs 66 μM α 94/98E, 0.26 mM Mg^{2+}, 7 μL additions (○); 1.02 mM Ca^{2+} vs 66 μM α 94/98E, 0.51 mM Mg^{2+}, 7 μL additions (□); 1.02 mM Ca^{2+} vs 66 μM α 94/98E, 1.03 mM Mg^{2+}, 7 μL additions (△); and (G) 2.05 mM Mg^{2+} vs 64 μM α 94/98E, 7 μL additions (○); 2.05 mM Mg^{2+} vs 64 μM α 94/98E, 55 μM EDTA, 7 μL additions (□). (B) Residuals for panel A. (D) Residuals for panel C. (F) Residuals for panel E. (H) Residuals for panel G. Residuals were scaled to the largest injection heat in each data set.

Table 4: Dependence of α 94/98E Thermal Stability on Na^+ Concentration

$[Na^+]$ (M)	T_m (K)	ΔH_u (kcal/mol)
0.14	314.8 ± 0.1	54.5 ± 0.3
0.24	316.3 ± 0.1	58.3 ± 0.3
0.34	317.9 ± 0.1	60.4 ± 0.3
0.44	318.6 ± 0.1	58.8 ± 0.3
0.64	321.1 ± 0.1	61.9 ± 0.3

the point obtained at a Na^+ concentration of 0.64 M lies well above the line defined by the data collected at lower concentrations.

The instantaneous slope of this plot, $dT_m/d(\ln[Na^+])$, is proportional to the stoichiometry of Na^+ binding, as indicated by the equation

$$\Delta n_{Na^+} = (\Delta H_u/RT_m^2)[dT_m/d(\ln[Na^+])] \quad (4)$$

where ΔH_u is the enthalpy of unfolding, T_m is the melting temperature, and R is the gas constant (*33*). The data points in Figure 7B were fit to a second-order polynomial (solid line). The derivative of the best-fit line equals $2.56x + 7.14$, where x is the natural logarithm of the Na^+ concentration. At 0.24 M, evaluation of this expression yields a slope of 3.49. Multiplying this value by $\Delta H_u/RT_m^2$, where ΔH_u = 58.4 kcal/mol and T_m = 316.3, yields a stoichiometry of 1.03 ± 0.10. The linear fit to the data collected at Na^+ concentrations of ≤0.44 M affords a similar result, 1.01 ± 0.07. Thus, the apparent stoichiometry is identical, within the experimental error, to that of wild-type α (*19*), implying that the combined D94S and G98E mutations do not substantively alter Na^+ binding behavior.

Na^+ Binding Affinity. The energetics of divalent ion binding in Na^+ and K^+ solution are compared in Table 5. The affinity of 94/98 for Ca^{2+} is 1.9 kcal/mol more favorable at 25 °C in K^+-containing buffer, due to competition by Na^+ for the vacant metal ion-binding loops in the apoprotein. To extract an estimate for the Na^+ binding constant, synthetic Ca^{2+} binding data were produced using the Ca^{2+} binding constants measured in Na^+ and K^+ solution. These data were then subjected to Monte Carlo simulation as described in Materials and Methods, employing a model that explicitly includes the monovalent ion binding event.

The results of the simulation (Figure 9) suggest that Na^+ binds to the apoprotein, presumably at the CD site, with an association constant of 130 M^{-1} at 25 °C. This value is somewhat smaller than that reported for the wild-type protein (*14*), suggesting that the 94/98E mutations may have compromised the affinity for the monovalent ion. However, the wild-type analysis employed data collected at 5 °C, rather

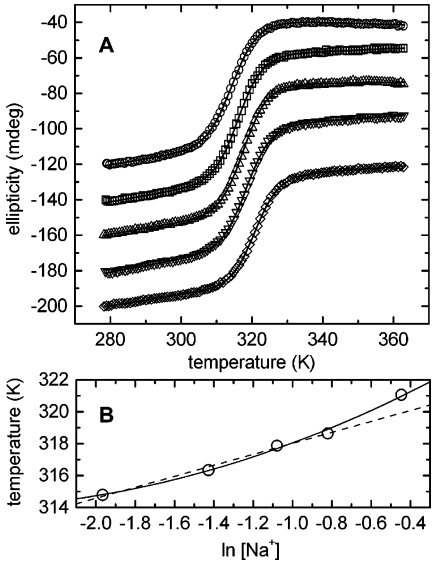

FIGURE 8: (A) Stability of α 94/98E as a function of Na^+ concentration. Thermal denaturation was monitored by circular dichroism at 222 nm, as described in Materials and Methods, at these total Na^+ levels: 0.14 (○), 0.24 (□), 0.34 (△), 0.44 (▽), and 0.64 M (◇). For clarity, only a subset of the data (every third point) has been displayed. The solid lines indicate the best least-squares fits to eq 3. (B) Stoichiometry of Na^+ binding. The apparent melting temperatures have been plotted vs the natural logarithm of the Na^+ concentration. The solid line represents the best fit to a second-order polynomial; the dashed line represents the best linear fit to the data gathered at Na^+ concentrations of ≤0.44 M.

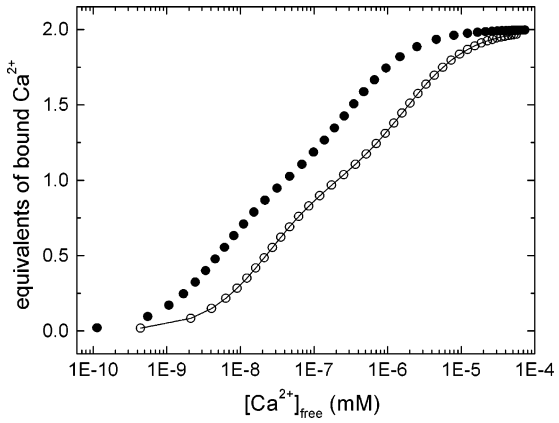

FIGURE 9: Estimation of the affinity of α 94/98E for Na^+. Synthetic binding data were produced using the apparent Ca^{2+} binding constants measured by ITC in K^+ and Na^+ solutions. These data were then simulated as described in Materials and Methods to find values of the Na^+ binding constants, K_{01} and K_{11}, that bring the curve corresponding to the data collected in K^+ (●) into agreement with the data collected in Na^+ (○). The solid line represents the best fit.

than 25 °C. As observed for wild-type α and the α S55D/E59D variant, the Na^+ binding data cannot be simulated without allowing for binding of Na^+ to the singly Ca^{2+}-bound form. The magnitude of K_{11}, 30 M^{-1}, suggests that Na^+ also competes weakly for the remaining vacant EF-hand.

DISCUSSION

The D94S and G98E (or G98D, in the case of rat *β*) mutations reproduce the CD-site coordination sphere in the local environment of the EF site. Conversely, the S55D and E59G (or D59G for rat *β*) mutations reproduce the EF-site coordination sphere in the environment of the CD site. The

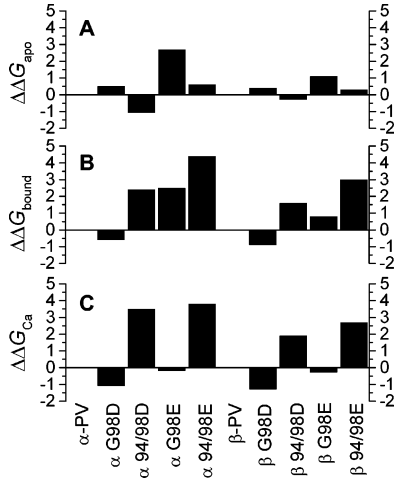

FIGURE 10: Changes in free energy resulting from relevant single mutations at residue 98 and simultaneous mutations at residues 94 and 98. (A) Changes in the stability of the apoprotein, determined by scanning calorimetry measurements published previously (*17*). (B) Inferred changes in the stability of the Ca^{2+}-bound protein. Values were obtained by recognizing that the change in the standard free energy change for Ca^{2+} binding is equal to the difference in the stabilities of the apo and bound states of the protein; i.e., $\Delta\Delta G_{Ca} = \Delta\Delta G_{bound} - \Delta\Delta G_{apo}$. (C) Measured changes in the overall standard free energy for Ca^{2+} binding.

preparation of these site-interconversion variants of the rat α and *β* isoforms was driven by a desire to examine the importance of context in the performance of these ligand arrays. The simultaneous mutations at residues 55 and 59 were found to have a minimal impact on divalent ion binding behavior. The engineered CD sites retained the phenotype of the wild-type CD sites: low affinity for *β* and high affinity for α. By contrast, the combined mutations at residues 94 and 98 markedly reduce the divalent ion affinity of the EF site in both isoforms. The work presented here was undertaken in an effort to identify the structural basis for the reduction in affinity. We begin the discussion by summarizing the energetics of divalent ion binding in the four 94/98 double variants: α D94S/G98E, α D94S/G98D, *β* D94S/G98D, and *β* D94S/G98E.

The standard Gibbs free energy change for Ca^{2+} binding corresponds to the difference in the energies of the protein in the free and bound states. The changes in the stabilities of the apo and Ca^{2+}-bound states of the relevant proteins are depicted graphically in Figure 10, along with the $\Delta\Delta G$ for Ca^{2+} binding. The actual numerical values for wild-type α and α 94/98E are listed in Table 5.

A priori, heightened electrostatic repulsion in the bound state offers a potential explanation for the reduced divalent ion affinity of the 94/98 variants. The presence of a negative charge at position 98 might be incompatible with the local electric field. The behaviors of the G98D(E) variants, however, are inconsistent with this hypothesis. The G98D mutations actually increase the Ca^{2+} affinity by 1.1 and 1.4 kcal/mol in rat α and *β*, respectively. These increases result from modest destabilization of the apoprotein, possibly due to heightened electrostatic repulsion, and modest stabilization of the bound state. The ligand array in the EF site of G98D is identical to that of the CD site in α S55D/E59D, which also exhibits a perceptible stabilization of the bound form. In that variant, the carboxylate of Asp-59 adopts a position immediately adjacent to the N-terminal end of the D helix,

Table 5: Divalent Ion Binding Energetics for Wild-Type α-PV and α D94S/G98E

			Ca^{2+} binding			Mg^{2+} binding		
protein	cation	T^a	$\Delta G_{total}{}^b$	ΔH_{total}	$-T\Delta S_{total}{}^c$	$\Delta G_{total}{}^b$	ΔH_{total}	$-T\Delta S_{total}{}^c$
α-PV[d]	Na^+	25	−22.0	−5.6	−16.4	−11.6	8.2	−19.7
	Na^+	5	−20.6	−5.5	−15.1	−10.0	9.4	−19.4
	K^+	5	−23.2	−7.9	−15.3	−12.6	6.7	−19.3
α D94S/G98E	Na^+	25	−18.2	−1.4	−16.8	−4.9[e]	4.8[e]	−9.7[e]
	K^+	25	−20.1	−19.6	−0.5	−8.8	−12.2	3.4

[a] Temperature in degrees Celsius. [b] Equal to $-RT \ln(k_1k_2)$, where R is the gas constant, T is the absolute temperature, and k_1 and k_2 are the binding constants for the first and second binding events, respectively. [c] Equal to $\Delta G - \Delta H$. [d] From ref *14*. [e] Value does not include any contribution by the low-affinity Mg^{2+}-binding site.

hydrogen bonding to the amide nitrogen of Glu-62 (*34*). This interaction and the concomitant stabilization of the D helical dipole may account for the increased stability of the bound form of α S55D/E59D and, by inference, the increased stability of the bound states of the α and β G98D variants.

Although the G98E mutations, in α and β, do not markedly increase Ca^{2+} affinity, neither do they antagonize it. In α, the apo and bound states are destabilized by 2.7 and 2.5 kcal/mol, respectively, producing a 0.2 kcal/mol improvement in the standard free energy for Ca^{2+} binding. In β, apo and bound states are destabilized by 1.1 and 0.8 kcal/mol, respectively, producing a 0.3 kcal/mol improvement in Ca^{2+} binding free energy. Presumably, the longer glutamyl side chain places the carboxylate closer to adjacent regions of negative charge, exacerbating electrostatic repulsion. The comparable destabilization of the apo and bound states suggests that, unlike the aspartyl side chain, the glutamyl side chain is unable to adopt a helix-stabilizing configuration in the bound state. To date, efforts to confirm this hypothesis have been frustrated by an inability to crystallize either α or β G98E.

Given that replacement of Gly-98 with glutamate or aspartate actually produces perceptible increases in Ca^{2+} affinity, the placement of a carboxylate side chain at position 98 is evidently not inimical to tight binding. However, if Asp-94 is replaced with serine in the context of the G98D-(E) mutations, a major reduction in divalent ion affinity is observed. The overall standard free energies for Ca^{2+} binding are 3.5 and 3.8 kcal/mol less favorable in the α 94/98D and α 94/98E variants, respectively. The attenuations observed for the corresponding β variants amount to 1.9 and 2.7 kcal/mol, respectively. It is evident from Figure 10 that the reduction in binding free energy in each case is largely due to the pronounced destabilization of the bound state. The 94/98D and 94/98E mutations actually have opposing effects on the apo form, with 94/98D producing modest stabilization and 94/98E producing modest destabilization.

Inspection of the relevant thermodynamic quantities (Table 5) indicates that the reduction in Ca^{2+} affinity has an enthalpic origin. The entropic contributions to the binding free energy are, in fact, somewhat more favorable for the 94/98 variants than for the wild-type proteins. Moreover, the enthalpic cost is associated with the second binding event, i.e., binding to the EF site. That event is actually endothermic for three of the four variants and only slightly exothermic for β 94/98D.

Conceivably, the unfavorable enthalpy change associated with binding of Ca^{2+} to the engineered EF site could be a consequence of suboptimal coordination geometry. However, the structural data do not support this hypothesis. As shown in Figure 3, the bond lengths and angles in the wild-type CD site and the engineered EF site in 94/98E are very similar, despite the 3.2 kcal/mol difference in the binding free energies of the two sites. In anticipation of the subsequent discussion, however, it should be noted that, whereas the liganding side chains at $+x$, $+y$, $+z$, and $-z$ are nearly superimposable, the configuration of the Glu-98 side chain in 94/98E departs perceptibly from that of Glu-59 in the wild-type CD site.

It would appear, then, that Ca^{2+} ligation is optimized in the engineered site and that the enthalpic cost is paid elsewhere in the molecule. Increased competition by Na^+ offered a potential explanation. The wild-type apoprotein binds 1 equiv of Na^+, and the monovalent ion is believed to occupy the CD site. Introduction of the CD-like ligand array into the EF site of 94/98E might have conferred heightened affinity for Na^+ at that site. Endothermic displacement of an additional equivalent of bound Na^+ would carry an enthalpic penalty. However, the dependence of the T_m for apo-94/98E on Na^+ concentration indicates a stoichiometry of 1.0, identical to that of wild-type α.

Careful inspection of the 94/98E structure reveals that the conformation of Phe-57 is altered relative to the wild-type protein (Figure 4). This shift in position apparently results from encroachment by the Glu-98 side chain and probably accounts for the displacement of the E98 side chain, relative to E59 in the CD site, observed in the crystal structure (Figure 3). The repositioning of the phenyl ring also exacerbates the close contact with the Ser-55 hydroxyl. These steric clashes may be responsible for the enthalpic penalty associated with the second divalent ion binding event. In rat β, Phe-57 is replaced with tyrosine. Presumably, however, the phenolic ring of Tyr-57 would also experience crowding, accounting for the qualitatively similar impact of the 94/98E mutations in the rat β background.

The γ-carboxylate of Asp-98, if indirectly coordinated to the bound Ca^{2+}, would likewise necessitate reorientation of Phe-57. Thus, steric interference provides a plausible reason for the comparable reduction in affinity observed for both the 94/98E and 94/98D variants. The explanation, however, may not be this simple. Site 2 in troponin C has a ligand constellation identical to that of parvalbumin 94/98D, and it likewise displays a relatively low affinity for Ca^{2+}. However, the aspartate residue in that system corresponding to Asp-98 does not participate in coordination. Rather, it is positioned so that the carboxylate accepts a hydrogen bond from the backbone amide of residue $i + 3$. As a result, the $\beta-\gamma$ bond is directed away from the binding pocket, eliminating the possibility of steric interference. It may be premature, therefore, to conclude that the reduced divalent

ion affinities of the parvalbumin 94/98E and 94/98D variants have a common origin. Structural data for the parvalbumin 94/98D variant could provide insight into this issue.

Concluding Remarks. The replacement of Gly-98 alone, with either aspartate or glutamate, is not sufficient to diminish parvalbumin EF-site divalent ion affinity. Our previous structural analysis on α S55D/E59D would suggest that, in fact, the side chain of residue 98 does not participate in Ca^{2+} coordination in either G98D or G98E. However, replacement of Asp-94 with serine eliminates an anionic ligand. Thus, when the D94S mutation is superimposed on G98E, the carboxylate at residue 98 is recruited to the $-x$ position. The resulting coordination sphere is virtually indistinguishable from that of the CD site. However, optimization of Ca^{2+}−ligand bond lengths and bond angles carries a costly enthalpic price tag, requiring unfavorable contact between the C_γ atom of glutamate and Phe-57. It is evident that the parvalbumin EF site is not designed to harbor a coordinating side chain at residue 98.

REFERENCES

1. Bootman, M. D., Berridge, M. J., and Roderick, H. L. (2002) Calcium signalling: More messengers, more channels, more complexity, *Curr. Biol. 12*, R563−R565.
2. Berridge, M. J., Bootman, M. D., and Roderick, H. L. (2003) Calcium signalling: Dynamics, homeostasis and remodelling, *Nat. Rev. Mol. Cell Biol. 4*, 517−529.
3. Kretsinger, R. H. (1980) Structure and evolution of calcium-modulated proteins, *CRC Crit. Rev. Biochem. 8*, 119−174.
4. Kawasaki, H., and Kretsinger, R. H. (1995) Calcium-binding proteins 1: EF-hands, *Protein Profile 1*, 297−490.
5. Celio, M. R., Pauls, T., and Schwaller, B. (1996) *Guidebook to the Calcium-binding Proteins*, Oxford University Press, New York.
6. Heizmann, C. W., and Kagi, U. (1989) Structure and function of parvalbumin, *Adv. Exp. Med. Biol. 255*, 215−222.
7. Pauls, T. L., Cox, J. A., and Berchtold, M. W. (1996) The Ca^{2+}-binding proteins parvalbumin and oncomodulin and their genes: New structural and functional findings, *Biochim. Biophys. Acta 1306*, 39−54.
8. Kretsinger, R. H., and Nockolds, C. E. (1973) Carp muscle calcium-binding protein. II. Structure determination and general description, *J. Biol. Chem. 248*, 3313−3326.
9. Goodman, M., and Pechere, J. F. (1977) The evolution of muscular parvalbumins investigated by the maximum parsimony method, *J. Mol. Evol. 9*, 131−158.
10. Nakayama, S., Moncrief, N. D., and Kretsinger, R. H. (1992) Evolution of EF-hand calcium-modulated proteins. II. Domains of several subfamilies have diverse evolutionary histories, *J. Mol. Evol. 34*, 416−448.
11. Fohr, U. G., Weber, B. R., Muntener, M., Staudenmann, W., Hughes, G. J., Frutiger, S., Banville, D., Schafer, B. W., and Heizmann, C. W. (1993) Human α and *β* parvalbumins. Structure and tissue-specific expression, *Eur. J. Biochem. 215*, 719−727.
12. Epstein, P., Means, A. R., and Berchtold, M. W. (1986) Isolation of a rat parvalbumin gene and full length cDNA, *J. Biol. Chem. 261*, 5886−5891.
13. Gillen, M. F., Banville, D., Rutledge, R. G., Narang, S., Seligy, V. L., Whitfield, J. F., and MacManus, J. P. (1987) A complete complementary DNA for the oncodevelopmental calcium-binding protein, oncomodulin, *J. Biol. Chem. 262*, 5308−5312.
14. Henzl, M. T., Larson, J. D., and Agah, S. (2004) Influence of monovalent cation identity on parvalbumin divalent ion-binding properties, *Biochemistry 43*, 2747−2763.
15. Kauffman, J. F., Hapak, R. C., and Henzl, M. T. (1995) Interconversion of the CD and EF sites in oncomodulin. Influence on the Eu^{3+} $^7F_0 \rightarrow {}^5D_0$ excitation spectrum, *Biochemistry 34*, 991−1000.
16. Henzl, M. T., Hapak, R. C., and Likos, J. J. (1998) Interconversion of the ligand arrays in the CD and EF sites of oncomodulin. Influence on Ca^{2+}-binding affinity, *Biochemistry 37*, 9101−9111.
17. Henzl, M. T., Agah, S., and Larson, J. D. (2004) Rat α- and *β*-parvalbumins: Comparison of their pentacarboxylate and site-interconversion variants, *Biochemistry 43*, 9307−9319.
18. Henzl, M. T., and Graham, J. S. (1999) Conformational stabilities of the rat α- and *β*-parvalbumins, *FEBS Lett. 442*, 241−245.
19. Henzl, M. T., Larson, J. D., and Agah, S. (2000) Influence of monovalent cations on rat α- and *β*-parvalbumin stabilities, *Biochemistry 39*, 5859−5867.
20. Haner, M., Henzl, M. T., Raissouni, B., and Birnbaum, E. R. (1984) Synthesis of a new chelating gel: Removal of Ca^{2+} ions from parvalbumin, *Anal. Biochem. 138*, 229−234.
21. Henzl, M. T., Agah, S., and Larson, J. D. (2004) Association of the AB and CD-EF domains from rat α- and *β*-parvalbumin, *Biochemistry 43*, 10906−10917.
22. Matthews, B. W. (1968) Solvent content of protein crystals, *J. Mol. Biol. 33*, 491−497.
23. Otwinowski, Z., and Minor, W. (1997) Processing of X-ray diffraction data collected in oscillation mode, *Methods Enzymol. 276*, 307−326.
24. French, G. S., and Wilson, K. S. (1978) On the treatment of negative intensity observations, *Acta Crystallogr. A34*, 517−525.
25. Collaborative Computational Project Number 4 (1994) The CCP4 Suite: Programs for Protein Crystallography, *Acta Crystallogr. D50*, 760−763.
26. Brünger, A. T., Adams, P. D., Clore, G. M., DeLano, W. L., Gros, P., Grosse-Kunstleve, R. W., Jiang, J. S., Kuszewski, J., Nilges, M., Pannu, N. S., Read, R. J., Rice, L. M., Simonson, T., and Warren, G. L. (1998) Crystallography & NMR system: A new software suite for macromolecular structure determination, *Acta Crystallogr. D54*, 905−921.
27. Bottoms, C. A., Schuermann, J. P., Agah, S., Henzl, M. T., and Tanner, J. J. (2004) Crystal structure of rat α-parvalbumin at 1.05 angstrom resolution, *Protein Sci. 13*, 1724−1734.
28. Winn, M. D., Isupov, M. N., and Murshudov, G. N. (2001) Use of TLS parameters to model anisotropic displacements in macromolecular refinement, *Acta Crystallogr. D57* (Part 1), 122−133.
29. Jones, T. A., Zou, J.-Y., Cowan, S. W., and Kjeldgaard, M. (1991) Improved methods for building protein models in electron density maps and the location of errors in these models, *Acta Crystallogr. A47*, 110−119.
30. Henzl, M. T., Larson, J. D., and Agah, S. (2003) Estimation of parvalbumin Ca^{2+}- and Mg^{2+}-binding constants by global least-squares analysis of isothermal titration calorimetry data, *Anal. Biochem. 319*, 216−233.
31. Pace, C. N., Hebert, E. J., Shaw, K. L., Schell, D., Both, V., Krajcikova, D., Sevcik, J., Wilson, K. S., Dauter, Z., Hartley, R. W., and Grimsley, G. R. (1998) Conformational stability and thermodynamics of folding of ribonucleases Sa, Sa2, and Sa3, *J. Mol. Biol. 279*, 271−286.
32. Engh, R. A., and Huber, R. (1991) Accurate bond and angle parameters for X-ray protein structure refinement, *Acta Crystallogr. A47*, 392−400.
33. Alberty, R. A. (1969) Maxwell relations for thermodynamic quantities of biochemical reactions, *J. Am. Chem. Soc. 91*, 3899−3903.
34. Lee, Y. H., Tanner, J. J., Larson, J. D., and Henzl, M. T. (2004) Crystal structure of a high-affinity variant of rat α-parvalbumin, *Biochemistry 43*, 10008−10017.
35. Laskowski, R. A., MacArthur, M. W., Moss, D. S., and Thornton, J. M. (1993) PROCHECK: A program to check the stereochemical quality of protein structures, *J. Appl. Crystallogr. 26*, 283−291.
36. DeLano, W. L. (2002) *The PyMOL Molecular Graphics System*, DeLano Scientific, South San Francisco, CA.

BI050770T